ELSEVIER

Nuclear Engineering and Design 189 (1999) 139–161

Nuclear Engineering and Design

On the regimes of premixing

S. Angelini, T.G. Theofanous *, W.W. Yuen

Department of Chemical and Nuclear Engineering, Center for Risk Studies and Safety, University of California, Santa Barbara, Santa Barbara, CA 93106, USA

Received 24 August 1998; accepted 24 November 1998

Abstract

The conditions of the MAGICO-2000 experiment are extended to more broadly investigate the regimes of premixing, and the corresponding internal structures of mixing zones. With the help of the data and numerical simulations using the computer code PM-ALPHA, we can distinguish extremes of behavior dominated by inertia and thermal effects—we name these the inertia and thermal regimes, respectively. This is an important distinction that should guide future experiments aimed at code verification in this area. Interesting intermediate behaviors are also delineated and discussed. © 1999 Elsevier Science S.A. All rights reserved.

1. Introduction

It is now well understood that large-scale steam explosions are highly dynamic events of propagative character. The media that support such propagations are called premixtures, and they are characterized by the volume fractions and length scales of their constituents—melt, liquid coolant, and vapor. Premixing is called the process that leads to the formation of premixtures, and it is a highly transient, generally multidimensional process governed by intense multiphase interactions (although mild by comparison to the propagation itself). As a key step in developing the proper understanding and predictive capability, starting with the MAGICO experiment (Angelini et al., 1992), premixing has been studied with the help of solid particle clouds. This focus on multifield aspects removes a key unknown, the melt length scale, and with well-defined initial and boundary conditions, allows unambiguous comparisons to predictive models. Perhaps more importantly this approach allows for a systematic variation of the experimental condition, so as to exercise the predictive tools, at the fundamental level, over wide ranges of conditions. This approach was continued with the MAGICO-2000 experiments, and more recently with the QUEOS and BILLEAU experiments in Germany and France, respectively. The MIXA experiments, which opened the way, together with MAGICO, employed pre-broken-up thermitic melts, and thus they were also guided to a large extent by similar considerations (Fletcher and Denham, 1993). How to build towards including break-up on this basis has been discussed and demonstrated in connection with specifying

* Corresponding author. Tel.: +1-805-8934900; fax: +1-805-8934927.

E-mail address: theo@theo.ucsb.edu (T.G. Theofanous)

PII: S0029-5493(99)00031-X

and using (for reactor assessment) the PM-ALPHA code (Theofanous et al., 1997a,b).

The present work is continuing the efforts on the multifield aspects. *Our main purpose is to introduce the notion of 'premixing regimes'*. Specifically, with the help of advanced MAGICO-2000 tests and PM-ALPHA calculations, we distinguish extremes of behavior dominated by inertia and thermal effects. We name these '*inertial*' and '*thermal premixing regimes*', respectively, and expect them to provide an important additional anchor in planning future experiments and assessing completeness of code verification efforts.

2. Preliminary considerations

As described previously (Angelini et al., 1995), PM-ALPHA calculations under cold MAGICO-2000 conditions revealed a plunger-like action—that is, deep cavities or 'holes' in the liquid pool forming just behind the descending cloud and closing up a short time later. The volume fraction of solids in the cloud, before entering the water, was $\sim 10\%$ and MAGICO-2000 experiments confirmed these predictions. This 'plunger' effect is even more pronounced in the QUEOS experiments, where the mode of particle delivery produces very dense ('lumps') particle clouds with volume fractions of $\sim 17\%$. Here, the length of the clouds is rather short (~ 30 cm), the water pools are saturated at the top and subcooled due to gravity head, and they are subcooled further due to self-pressurization, and the steaming appears as a short burst coincident with the lifetime of the water 'hole' (~ 250 ms). Even with hot runs this is a heavily inertia dominated behavior, not really germane to the premixing process. PM-ALPHA calculations indicate that to avoid the inertia regime, the particle volume fraction must be reduced to just a few percent. In MAGICO-2000, the pours are longer (150 cm), and by comparison to QUEOS rather dilute ($\sim 2\%$), and this places them outside of the range of inertia dominated regimes. However, the corresponding pour duration is only ~ 0.33 s, and a purely thermally-dominated regime would have even lower particle volume fractions and, particularly, prolonged pour durations. These considerations lead to a special adaptor in the MAGICO-2000 facility and the experiments reported here. In these experiments, we have achieved pours of $\sim 0.5\%$ particle volume fraction, ~ 6.5 m length and ~ 1.5 s pouring time, for a thermally-dominated behavior.

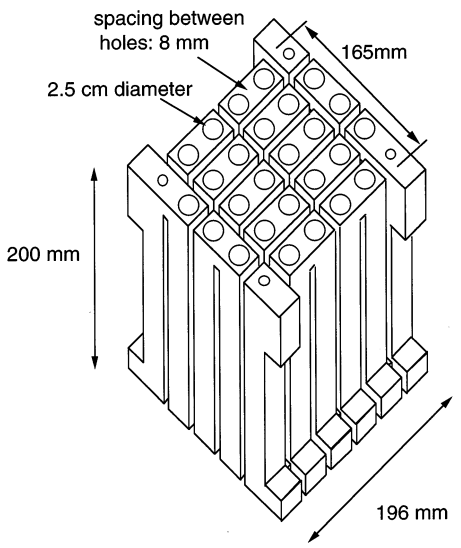

Fig. 1. The heating element in MAGICO-2000.

3. Experimental apparatus and measurement techniques

The MAGICO-2000 experiment has been described previously (Angelini et al., 1995). Its central component is the graphite heating element, illustrated in Fig. 1. It can deliver up to ~ 5 kg of ZrO_2 particles at temperatures up to ~ 2000°C. For the present experiment, this element was 'fitted' with a special device, such as to deliver the cloud at a much 'diluted' condition-volume fraction of 0.5%, pour length 6.5 m, pour duration 1.5 s. An overall view of the experimental stand, including key dimensions, is shown in Fig. 2. In the present experiments, for the interaction tank we employ a two-dimensional slab geometry, as illustrated in Fig. 3. The principal emphasis in measurements is placed in visualizing the internal structure of the whole premixing zone, and in

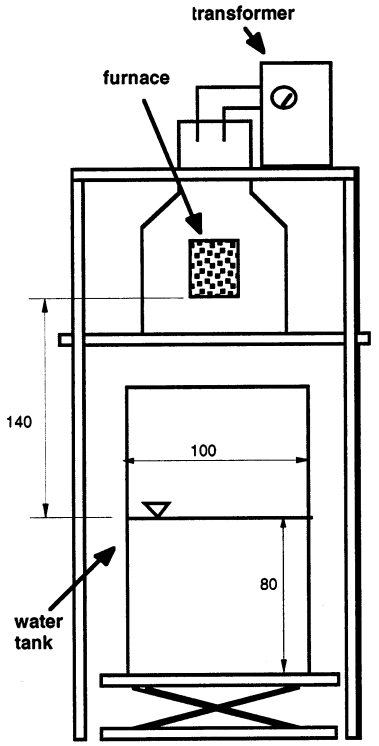

Fig. 2. Schematic of the MAGICO-2000 facility. All dimensions are in cm.

obtaining respective composition maps. This is done by radiography, employing flash X-rays, as explained in detail by Angelini and Theofanous (1997). With two film cassettes placed one on top of the other, we can map a 35×73 cm region, as illustrated in Fig. 3. Particle volume fractions are obtained by counting. In all regions of the film not occupied by particles the steam volume fractions are obtained from the film density and appropriate calibrations. The resolution is 200 dots per inch and the void fraction accuracy is estimated at $\pm 5\%$ (relative error).

4. Experimental results and interpretations

A total of eight experimental conditions were investigated, as summarized in Tables 1 and 2. The key point on these is that the ZrO_2 particulate volume fractions varied by about one order of magnitude. For the zero subcooling runs, saturation throughout was assured by boiling the water pool from below. In the following, code predictions will be shown alongside the presentation of experimental results. The code is the version documented by Theofanous et al. (1998) and the inputs for each run are according to the specifications given in Tables 1 and 2. Only the following additional clarifications are necessary:

1. The Cartesian geometry was modeled by matching exactly the dimensions of the tank. The pour area was modeled by matching its size in the direction of the tank width (the large dimension of the tank), and by spreading it over the entire depth of the 2D field (the small dimension of the tank). A 2×2 cm (runs in Table 1) and a 2.5×2.5 cm (runs in Table 2) numerical grid was used.

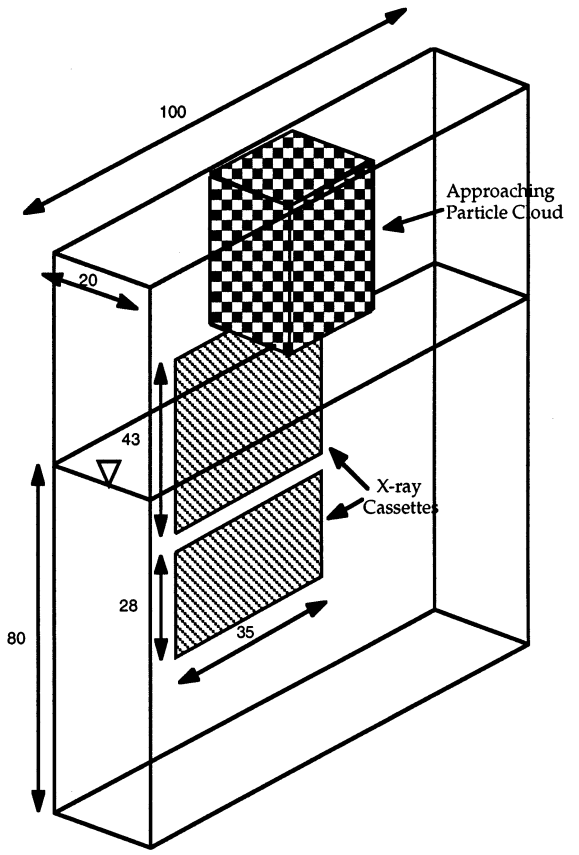

Fig. 3. Interaction tank and positions of X-ray cassettes. All dimensions are in cm.

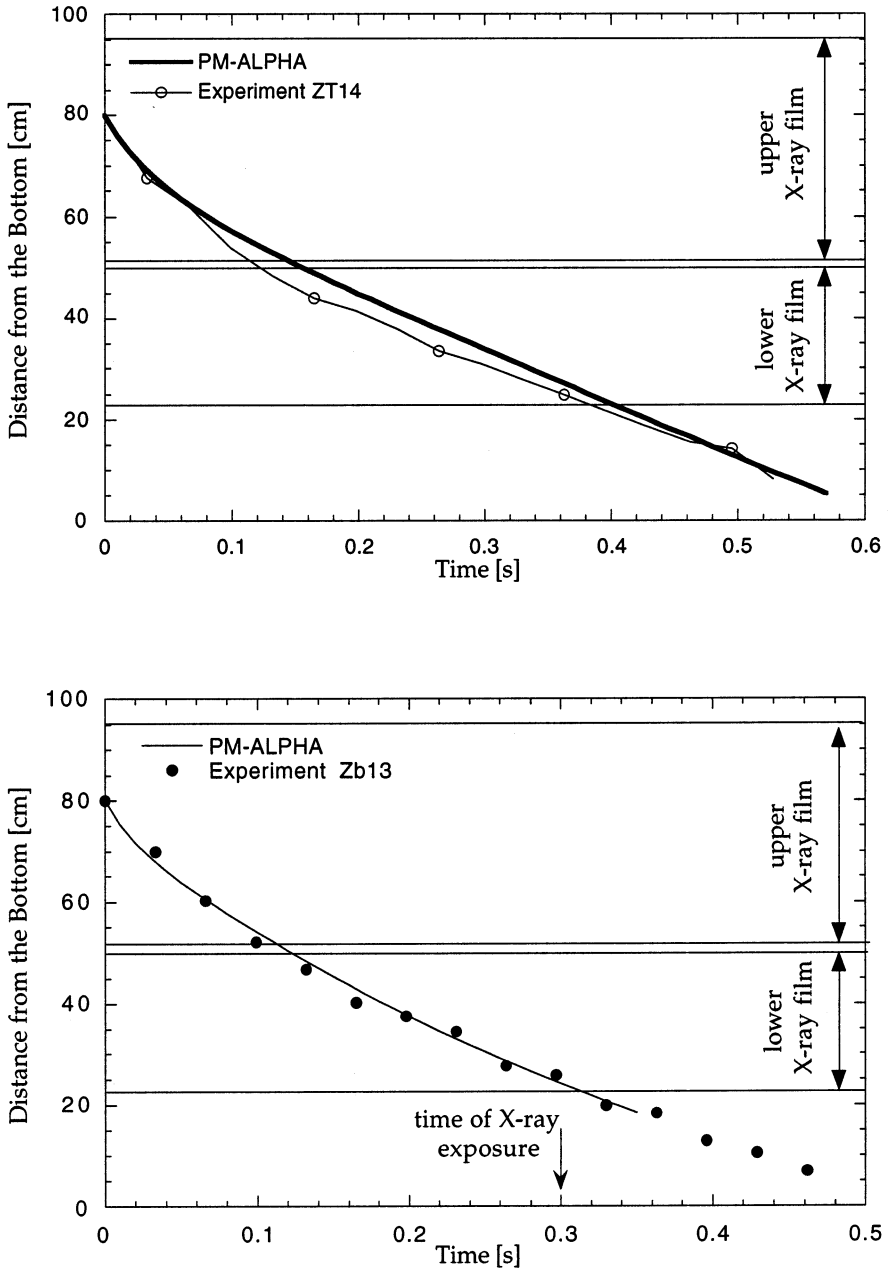

Fig. 4. Front advancement in two hot runs at 0.5% (top) and 5.5% (bottom) inlet particle volume fractions, and typical comparisons with PM-ALPHA predictions. Also shown are the regions covered by the two X-ray cassettes.

Table 1
Conditions for the cold MAGICO-2000 runs in a 2D slab geometry

Run	Particle size (mm)	Total mass (kg)	Particle volume fraction (%)	Impact velocity (m/s)	X-ray time (s)
ZCN	2	5.5	~6.5	~5.2	0.2, 0.25, 0.3, 0.35, 0.4
ZCT	7	5.0	~0.5	~4.4	0.1, 0.8

(a)

Fig. 5. Radiographs for runs ZCN. These are repeat runs and the five images (a)–(e) were obtained at times 0.2, 0.25, 0.3, 0.35 and 0.4 s following initial contact of the cloud with the water.

2. To determine more precisely the position of the fronts in the Eulerian calculation, we superposed Lagrangian tracer particles, made to move with the local (cell) velocity of the particulate field. As shown in Fig. 4, this approach does an excellent job in predicting the front advancement.

The five radiographic images taken for the conditions of run ZCN (this means five repeated runs under identical conditions) are shown in Fig. 5(a) through 5(e). The void fraction distributions deduced from the first three radiographs are shown in Fig. 6(a) through 6(c). We can clearly see the 'hole' described above and its closing at ~ 0.35 s. Notice the visualization detail as, for example, the 'clean' shapes of the upper cavity boundary, the highly structured lower portion of the cavity, and the fine detail on the hydrodynamic jet and its disintegration into spray, following collapse. PM-ALPHA predictions are shown in superposition to these radiographic images in Fig. 7(a) through 7(e). Note the 'wing' pattern of the particle distribution and the accurate depiction of the key void characteristics in the calculation. Also interesting to note is the exact matching of closing and timing and even shape of the emerging jet. Some numerical diffusion is present, as seen for the particles, and a small amount of void ($\sim 10\%$) retained below the liquid surface after closing (Fig. 7(c)).

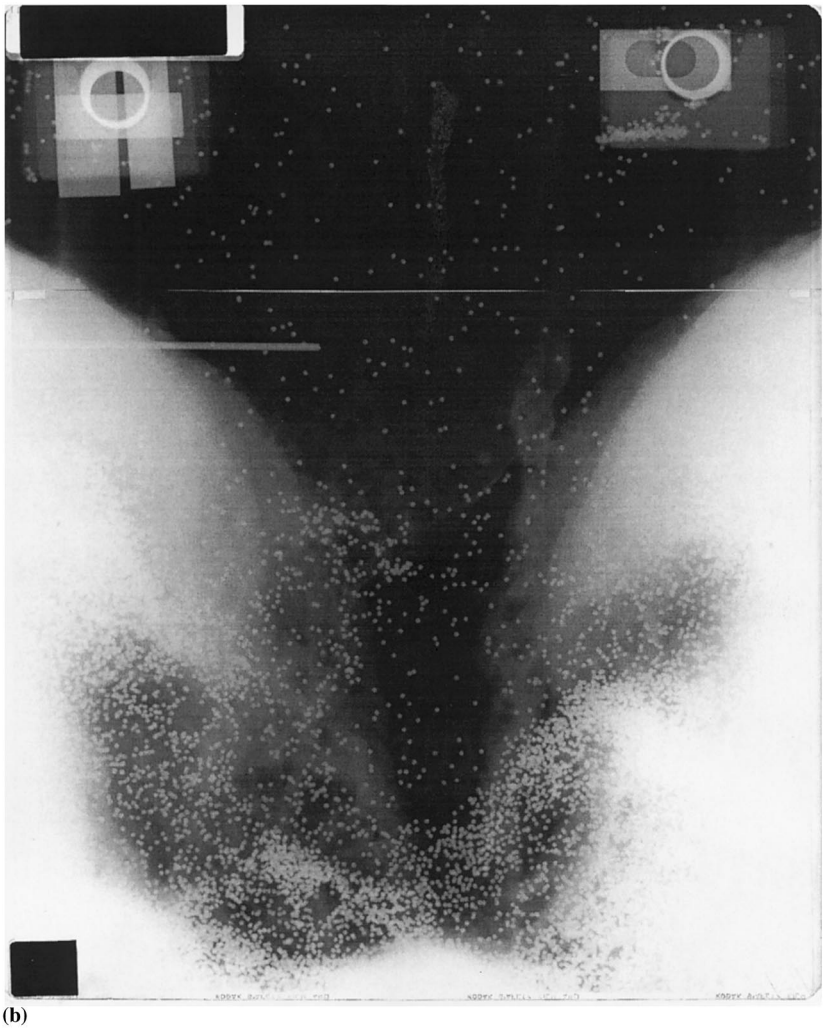

(b)

Fig. 5. (*Continued*)

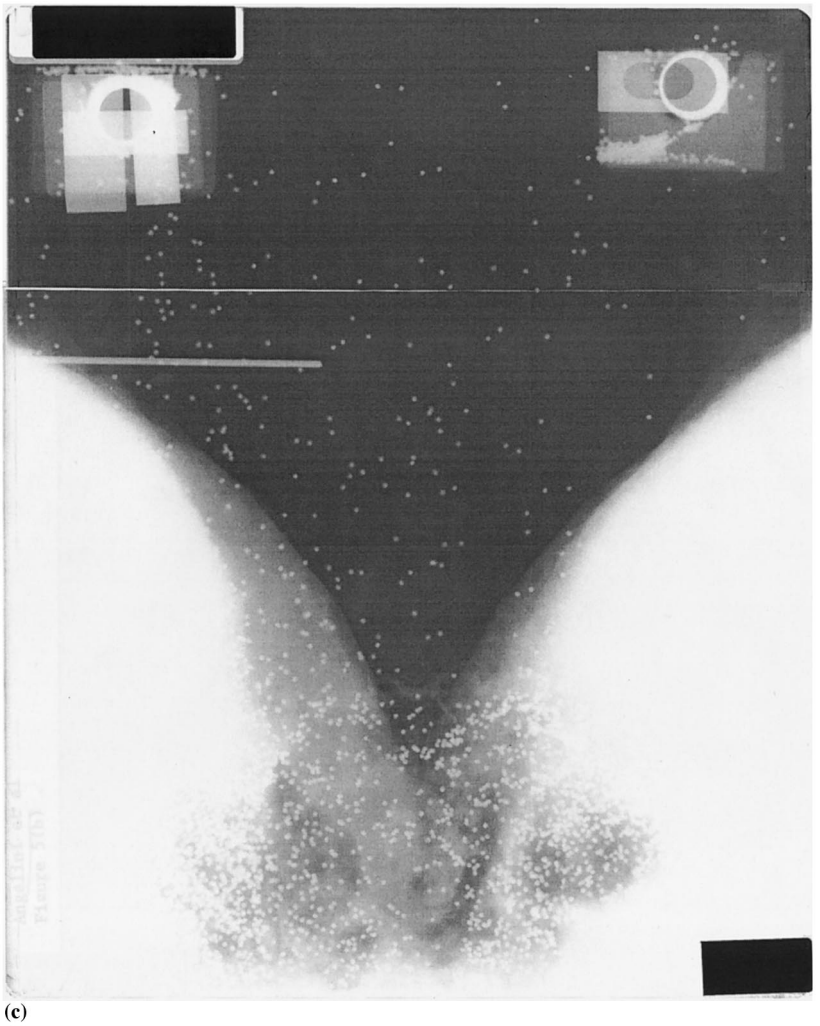

(c)

Fig. 5. (*Continued*)

The aim of the dilute pour runs was to avoid this inertia-dominated plunging regime, and this aim was achieved as illustrated with the results of runs ZCT in Fig. 8(a) through 8(c). Note in these figures the uniform particle cloud distribution in the air and the deceleration (increase in concentration) obtained in the water pool. We also see that a small amount of air, entrained with the particles, produces void fractions in the 10–20% range in the central portion of the mixing zone. Such small amounts of air are expected to be negligible under the strong steaming at hot run conditions.

The radiographs of the six hot runs conducted, under Table 2, are shown in Fig. 9(a) through 9(f). It is clear from 9(a) and 9(b) that the small particle runs produce highly voided regions (90–100%) even under 10°C subcooling, although in the latter case we see a more limited, in size, voided region. The void fraction maps for the other four, large particle runs are shown in Fig. 10(a) through 10(d). In the three dilute runs, the particle volume fractions in the mixing zone were found to be in the 0.6–1.1% range. It is interesting to note here the essential difference in regimes between Fig. 9(c) and 9(d). In Fig. 10(a′) and

10(b), we read corresponding void fractions in the 90–100% and 60–70% ranges. Also, it is interesting to note from Fig. 10(b), 10(c), and 10(d) that a change in particle temperature from 1650 to 2000°C does not appear to have a significant effect on the resulting premixtures. Numerical interpretations of these data are shown in Fig. 11(a) through 11(f). We find all the essential qualitative and quantitative features to be in excellent agreement. These include the location of the particle lower fronts and upper boundaries, the void fraction levels and the locations of sharp gradients, and the voided region pinch-off in the subcooled run. The effect of the temperature and particle size seems to be captured very well also in the calculations.

The last three runs in this series are idealized representations of what we wish to call the 'thermal regime' of premixing. As shown above, the behavior is not only quantitatively but also qualitatively different, and this difference becomes more vivid if the internal structures discussed above are viewed in the context of video records of the whole interaction vessel. Due to space limitations, this additional information will be presented in a future paper.

(d)

Fig. 5. (*Continued*)

(e)

Fig. 5. (*Continued*)

5. Conclusions

The conditions of the MAGICO-2000 experiment were extended to more broadly investigate the regimes of premixing and the corresponding internal structures of the mixing zones. With the help of the data and numerical simulations using the computer code PM-ALPHA, we could distinguish extremes of behavior dominated by inertial or thermal effects—we name these the inertial and thermal regimes of premixing, respectively. This is an important distinction that should guide future experiments aimed at code verification in this area.

Acknowledgements

This work was supported under the ROAAM program carried out for the US DOE's Advanced Reactor Severe Accident Program (ARSAP), under ANL subcontract No. 23572401 to UCSB.

Table 2
Conditions for the hot MAGICO-2000 runs in a 2D slab geometry

Run	Particle size (mm)	Total mass (kg)	Volume fraction (%)	Impact velocity (m/s)	Particle temperature (°C)	Water subcooling (°C)	X-ray time (s)
Z11	2	5.5	4.2	5.2	1550	0	0.3
Z12	2	5.7	4.2	5.2	1400	10	0.3
Zb13	7	4.8	5.5	5.2	1600	0	0.3
ZT14	7	5.1	0.5	4.4	1650	0	0.8
ZT15	7	4.4	0.5	4.4	1800	0	0.8
ZT16	7	2.6	0.5	4.4	2000	0	0.8

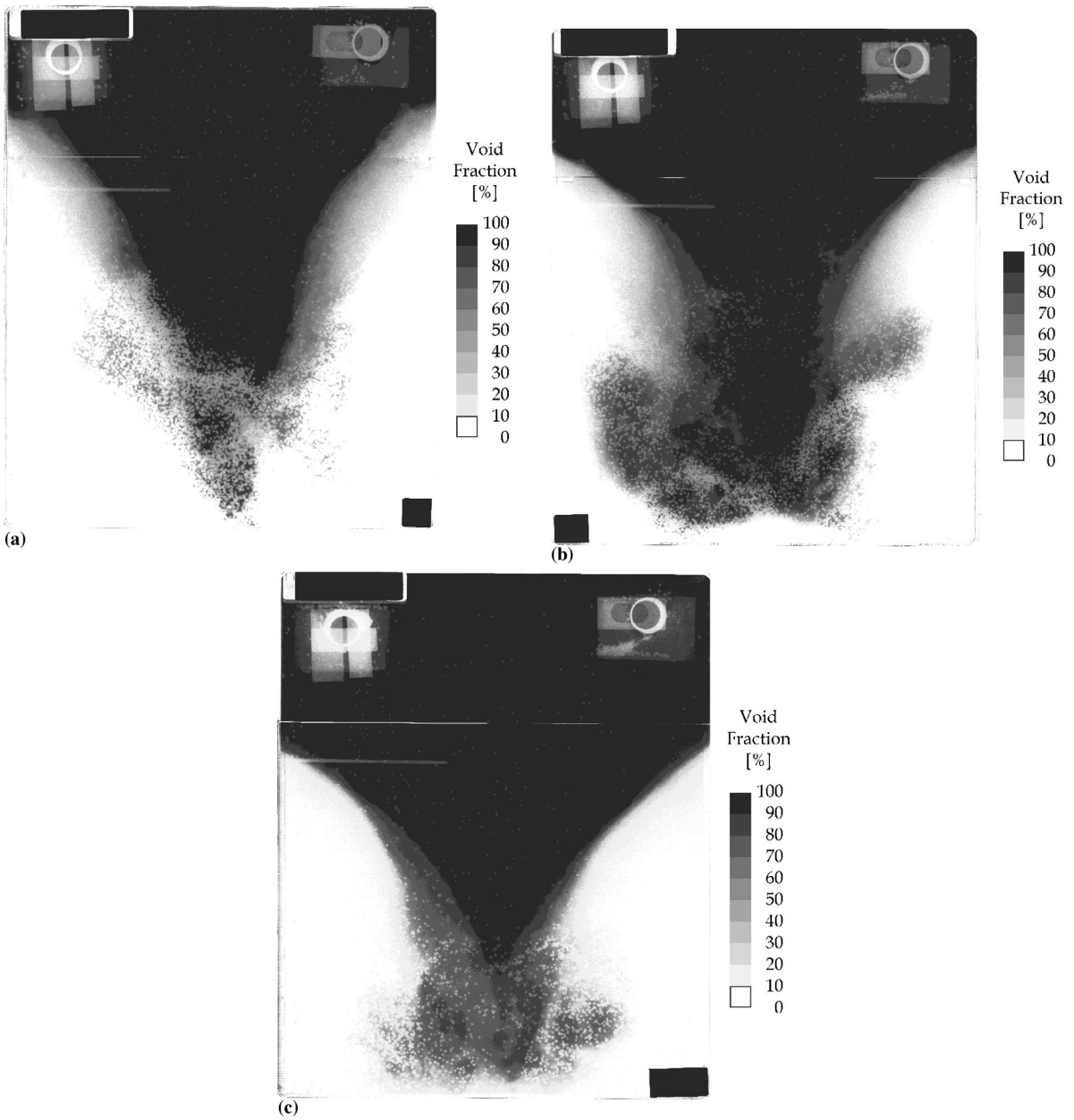

Fig. 6. Void fraction distributions deduced from the radiographs of Fig. 5. The (a) through (c) correspond to the (a) through (c) of Fig. 5.

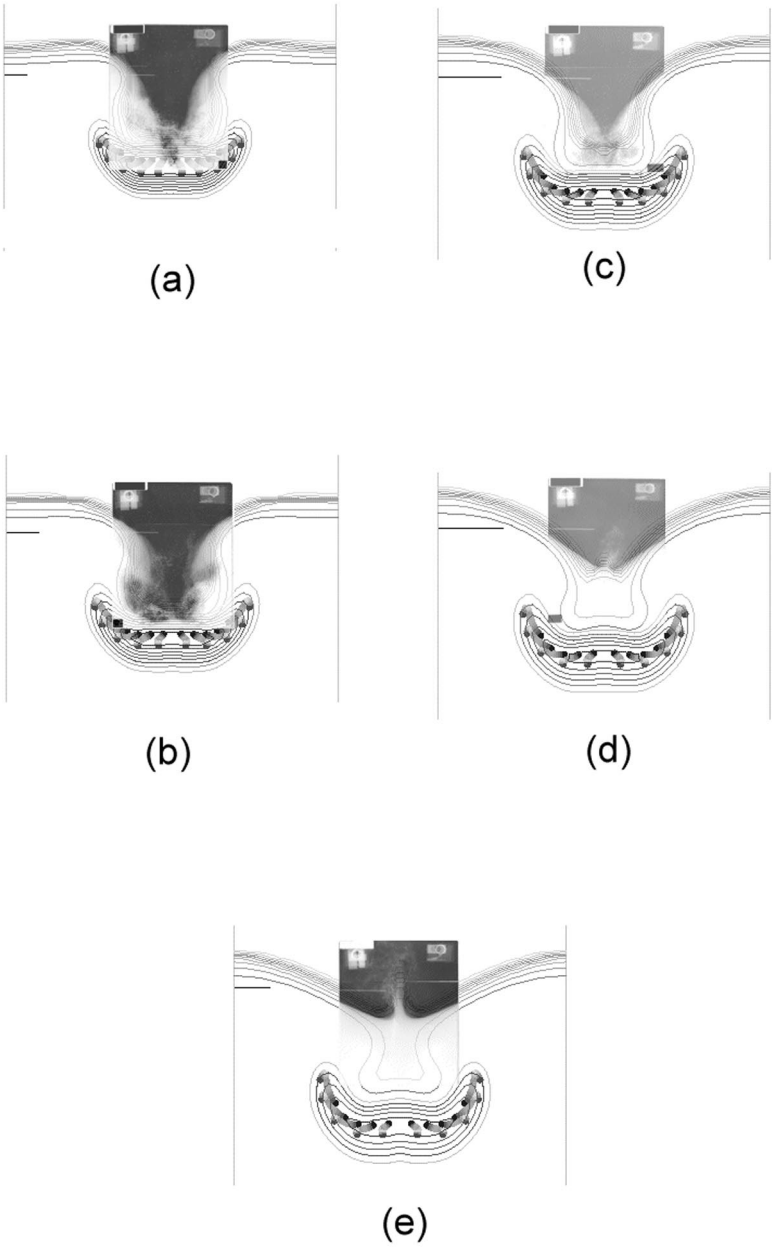

Fig. 7. PM-ALPHA predictions of the void fraction and particle distributions for the five ZCN runs. The (a) through (e) correspond to (a) through (e) of Fig. 5. Superposed also are the radiographic images.

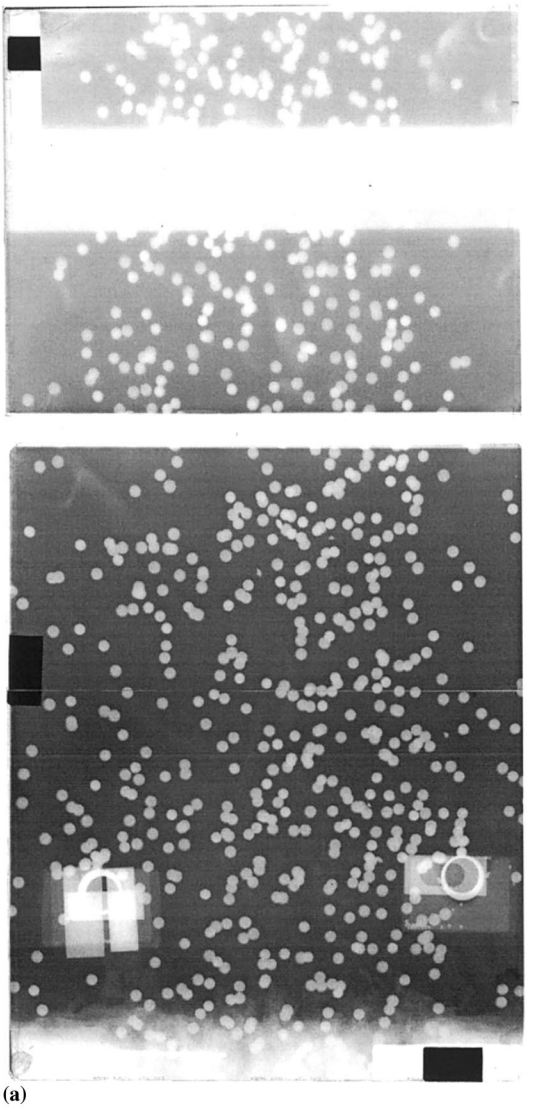

(a)

Fig. 8. Radiographs and deduced volume fraction distributions from runs ZCT: (a) image of a portion of the particle cloud in the air; (b) radiograph of the mixing region at 0.8 s following contact with water; and (c) quantified version of the radiograph in Fig. 8(b).

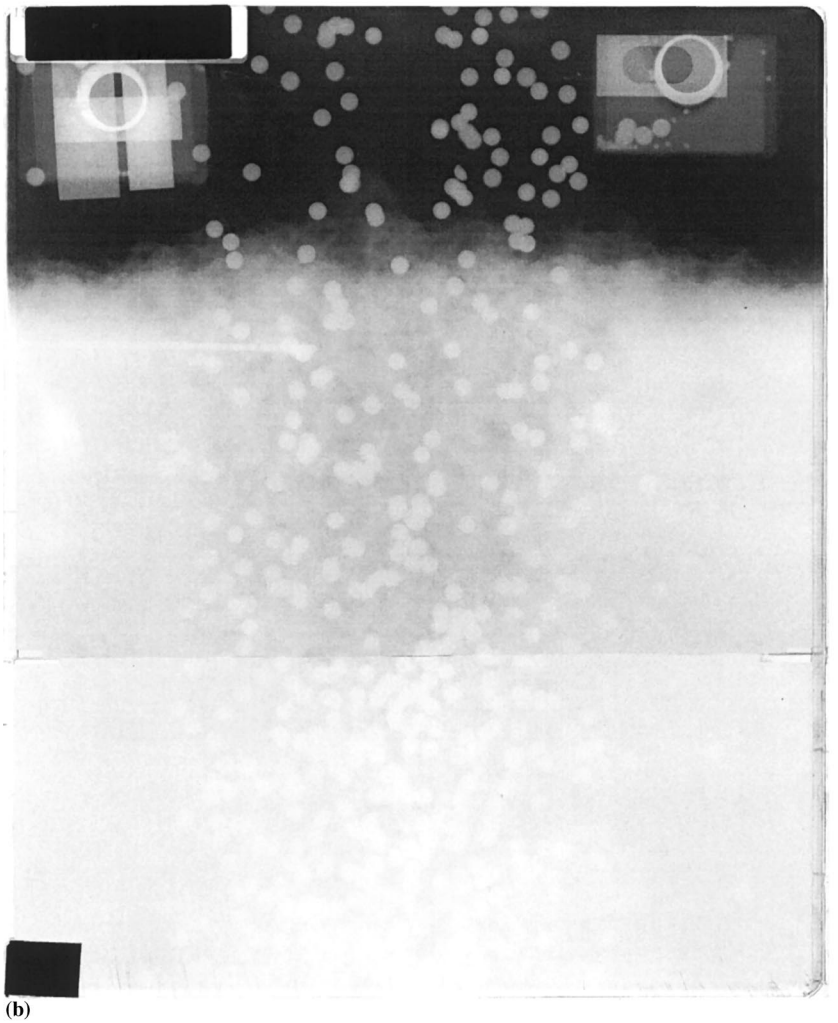

(b)

Fig. 8. (*Continued*)

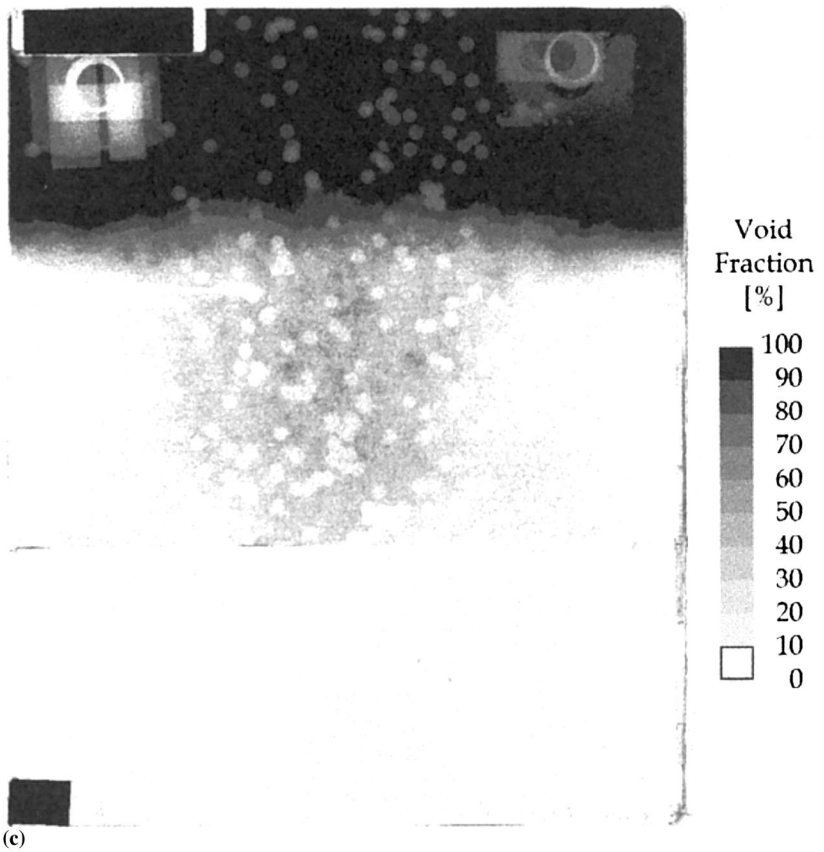

Fig. 8. (*Continued*)

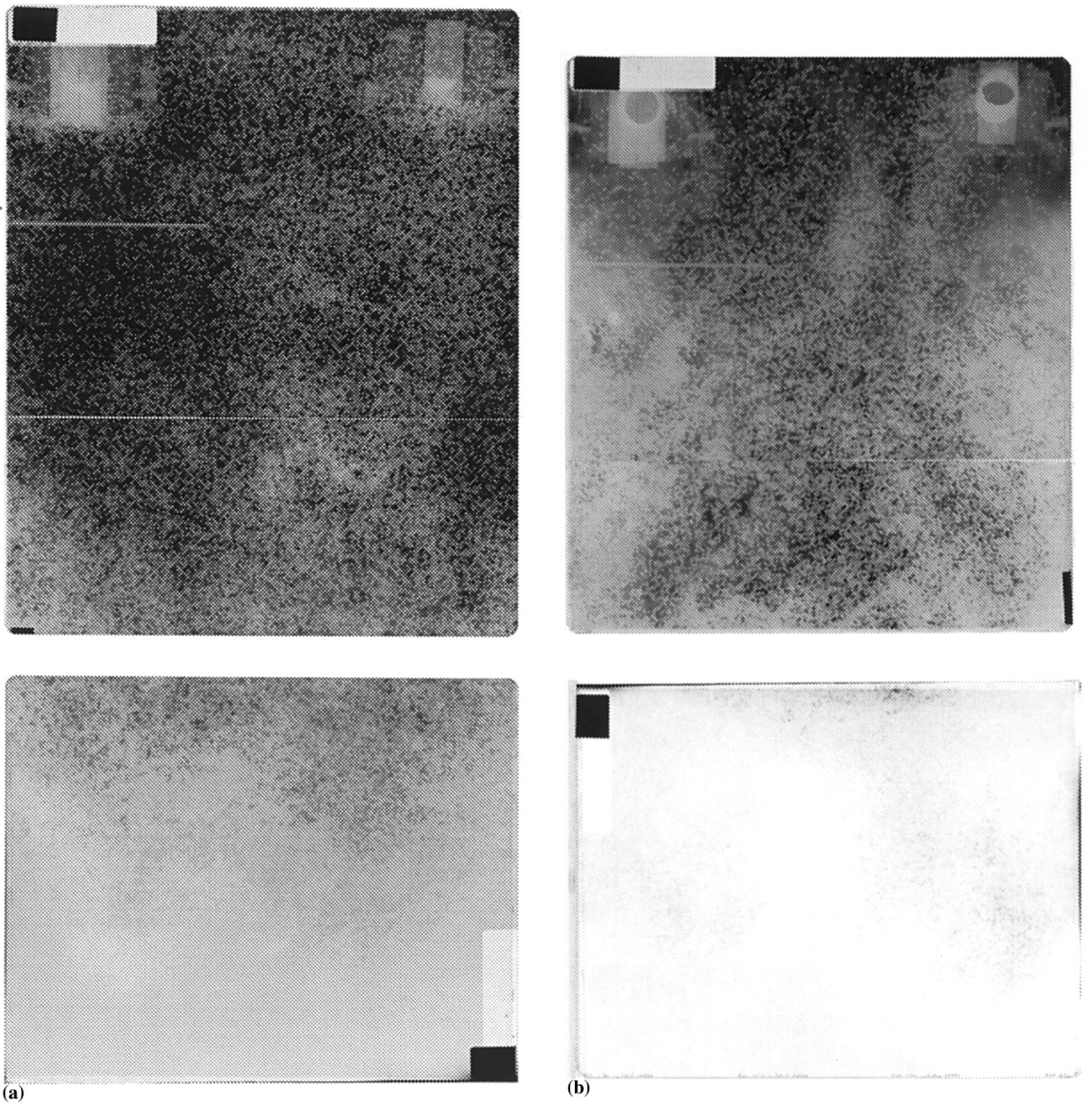

Fig. 9. The radiographs obtained in the runs of Table 2. The (a) through (f) correspond to runs 11 through 16 in the table.

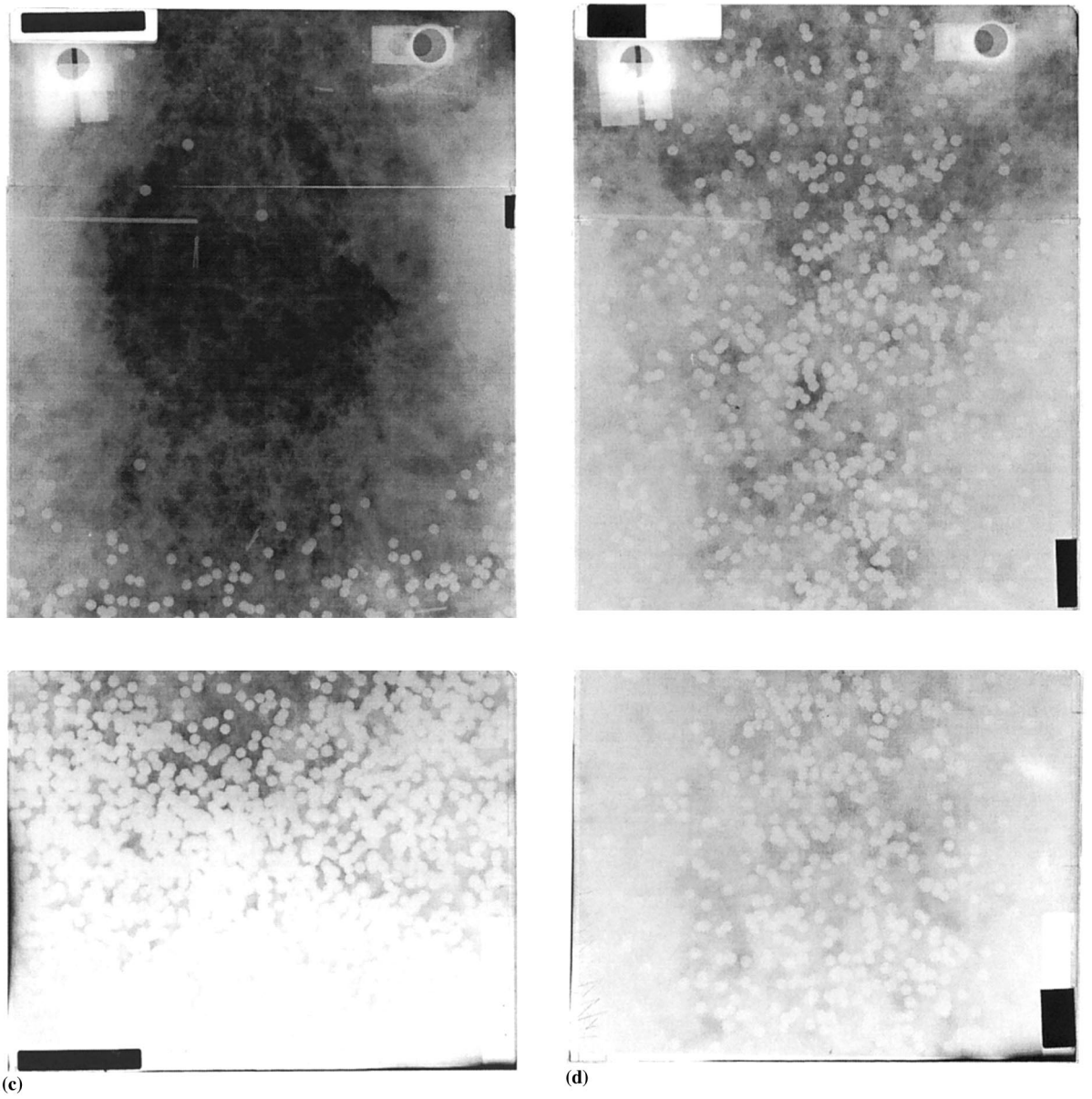

(c) (d)

Fig. 9. (*Continued*)

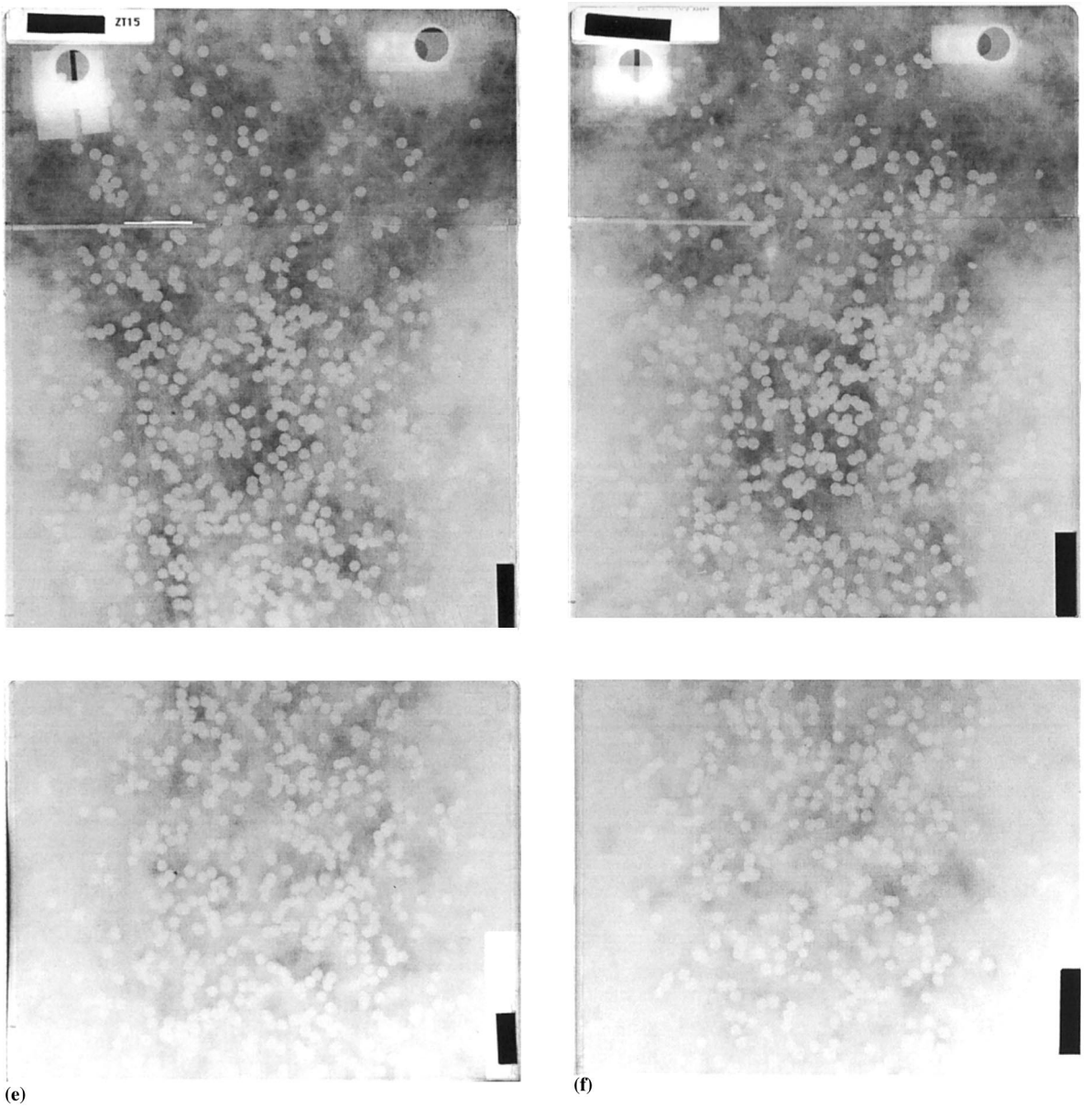

Fig. 9. (*Continued*)

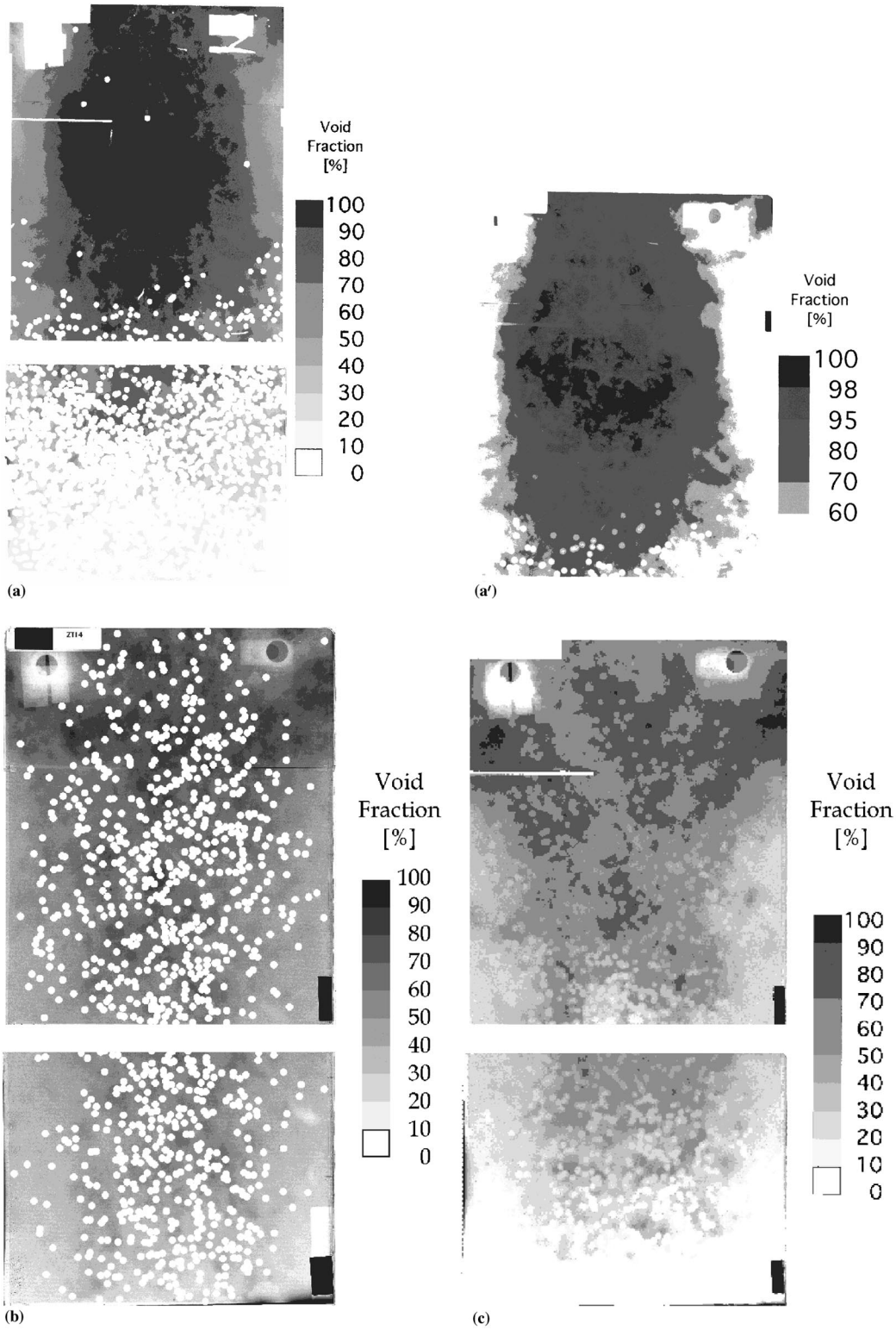

Fig. 10. Quantified images of the radiographs in Fig. 9. The (a) through (d) correspond to the (c) through (f) in Fig. 9. Fig. 10(a′) represents the upper film shown in Fig. 10(a), but scanned so as to emphasize the region of very high void fractions.

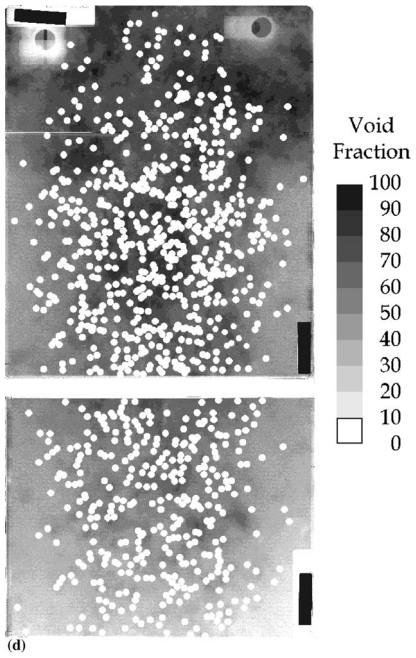

Fig. 10. (*Continued*)

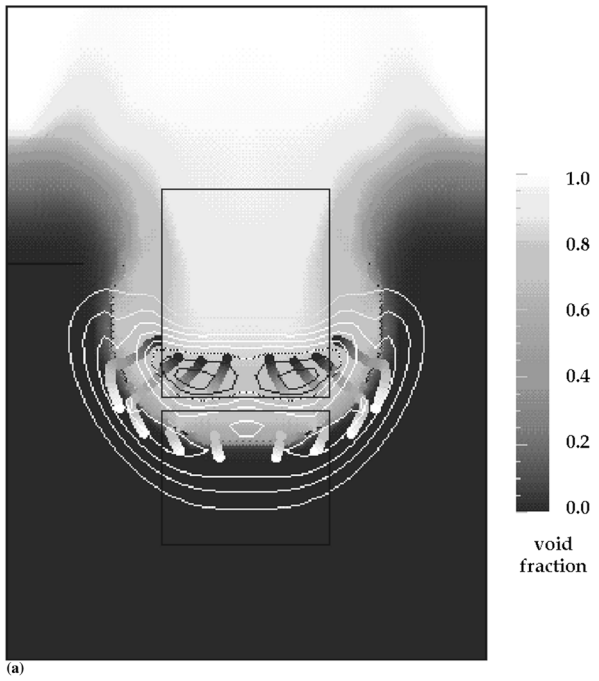

Fig. 11. (a) PM-ALPHA predictions of void fraction and particle volume fraction distributions at the time and conditions corresponding to radiographs of Fig. 9. Predicted particle volume fraction contour lines are from 0.5–4% in 0.5% interval. (b) Predicted particle volume fraction contour lines are from 1–6% in 0.5% interval. (c) Predicted particle volume fraction contour lines are from 0.5–3% in 0.5% interval. (d) The measured (from the radiographs) particle volume fraction distributions were in the 0.6–1.1% range. Predicted particle volume fraction contour lines are from 0.6–1.8% in 0.2% interval. (e) The measured (from the radiographs) particle volume fraction distributions were in the 0.6–1.1% range. Predicted particle volume fraction contour lines are from 0.6–2% in 0.2% interval. (f) The measured (from the radiographs) particle volume fraction distributions were in the 0.6–1.1% range. Predicted particle volume fraction contour lines are from 0.6–2% in 0.2% interval.

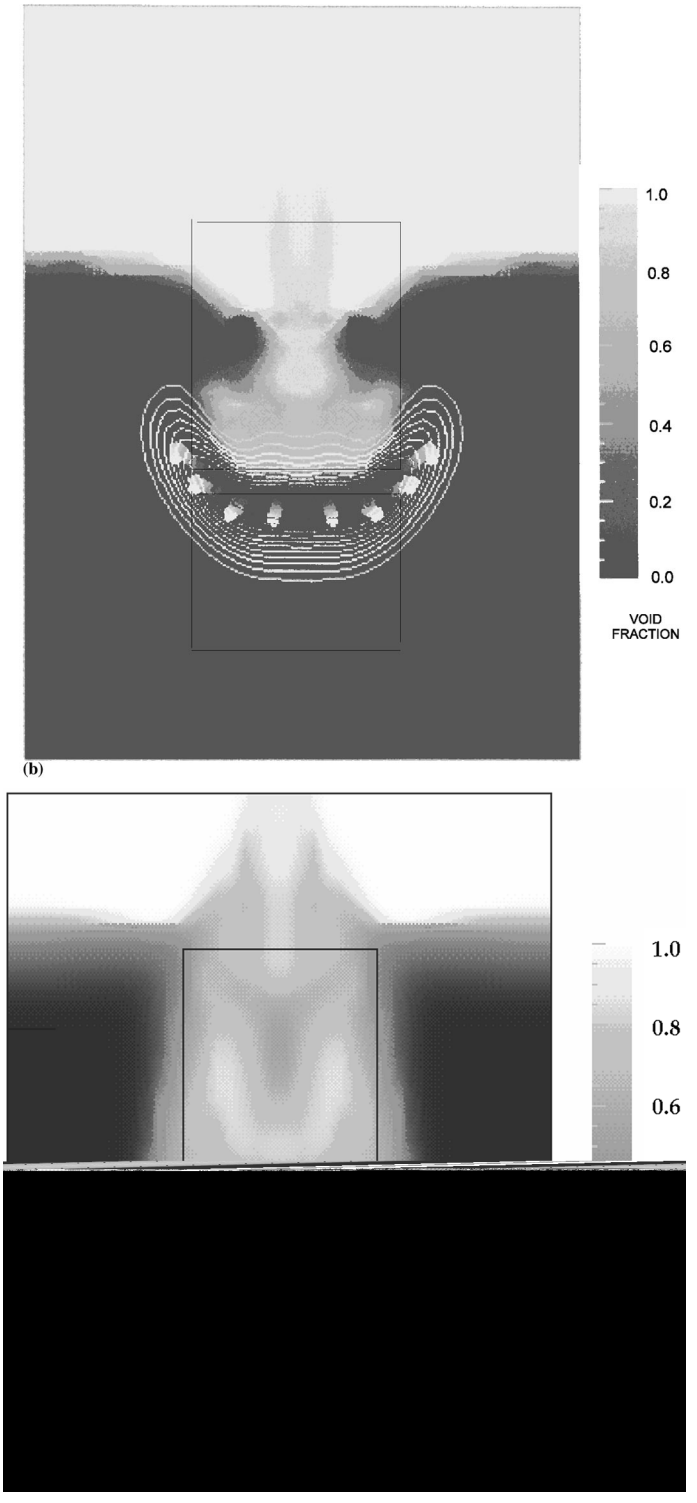

Fig. 11. (*Continued*)

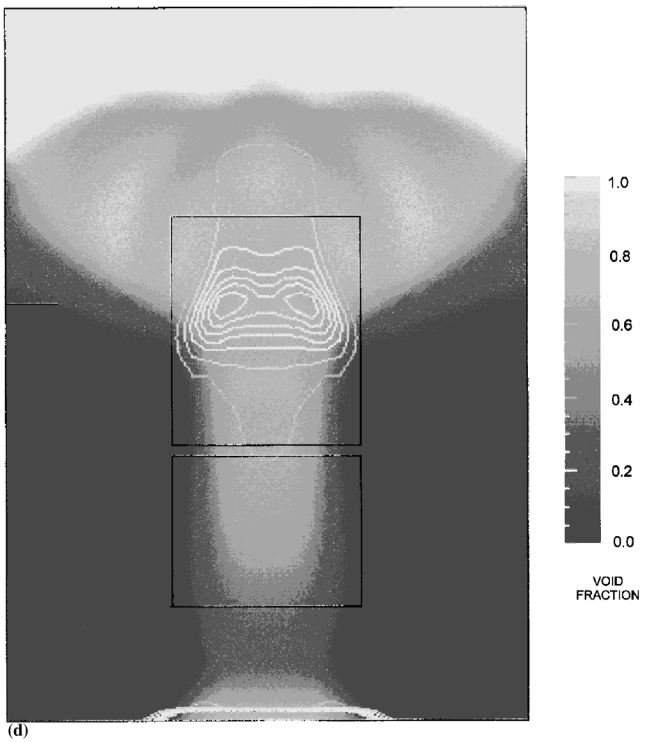

(d)

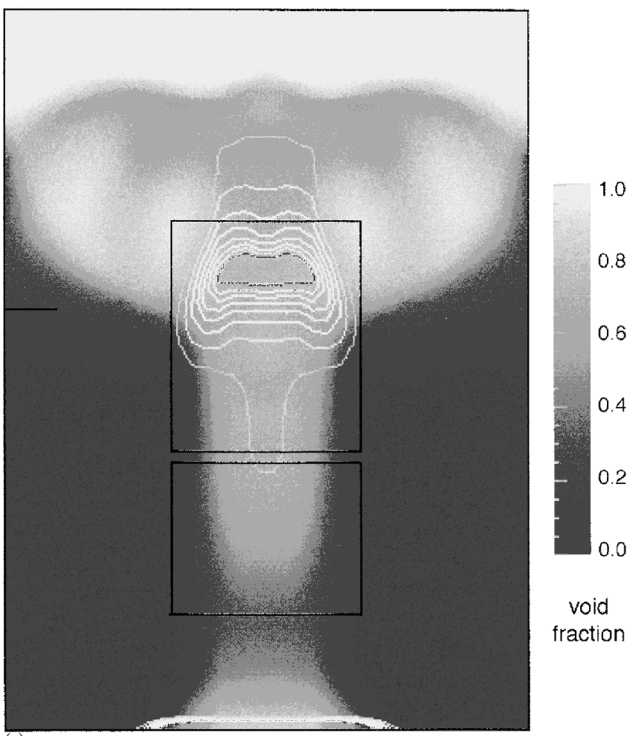

(e)

Fig. 11. (*Continued*)

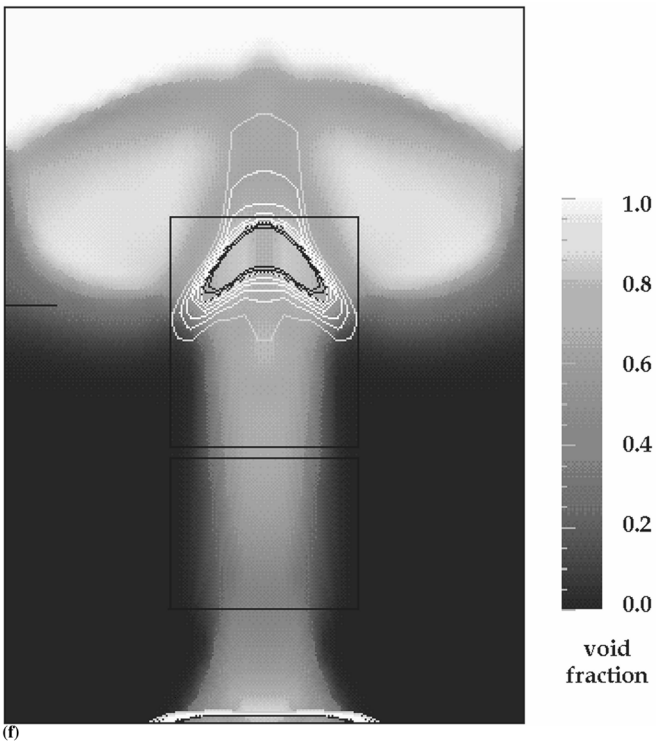

Fig. 11, (*Continued*)

References

Angelini, S., Takara, E., Yuen, W.W., Theofanous, T.G, 1992. Multiphase transients in the premixing of steam explosions. Proceedings of the 5th International Meeting on Nuclear Reactor Thermohydraulics, NURETH-5, Salt Lake City, UT, 21–24 September, Vol. II, pp. 471–478. (See also Nuclear Engineering and Design, 146, 83-95, 1994).

Angelini, S., Theofanous, T.G., Yuen, W.W., 1995. The mixing of hot particles clouds plunging into water. Proceedings of the 7th International Meeting on Nuclear Reactor Thermohydraulics, NURETH-7, Saratoga Springs, NY, September. Vol. 1, pp. 1754–1778, (see also Nuclear Engineering and Design, 177, 285-301, 1997).

Angelini, S., Theofanous, T.G., 1997. Void fraction measurements by means of flash X-ray radiography. OECD/CSNI Specialists Meeting on Advanced Instrumentation and Measurement Techniques, Santa Barbara, CA, 17–20 March.

Fletcher, D.F., Denham, M.K., 1993. Validation of the CHYMES mixing model. Proceedings of the CSNI Specialists Meeting on Fuel–Coolant Interactions, Santa Barbara, CA, 5–8 January (NUREG/CP-0127, March 1994, 89).

Theofanous, T.G., Yuen W.W., Angelini, S., 1998. Premixing of steam explosions: PM-ALPHA verification studies. DOE/ID-10504, June.

Theofanous, T.G., Yuen, W.W., Angelini, S., 1997a. The verification basis of the PM-ALPHA code. OECD/CSNI Specialist Meeting on Fuel–Coolant Interactions, Jaeri, Tokai, Japan, 19–21 May, pp. 219–268.

Theofanous, T.G., Yuen, W.W., Angelini, S., Sienicki, J.J., Freeman, K., Chen, X. Salmassi, T., 1997b. Lower head integrity under steam explosion loads. OECD/CSNI Specialist Meeting on Fuel–Coolant Interactions, Jaeri, Tokai, Japan, 19–21 May, pp. 63–118.